JOURNAL OF Materials CHEMISTRY

The functionalization of titanium with EDTA to induce biomimetic mineralization of hydroxyapatite

Chuanbin Mao,* Hengde Li, Fuzhai Cui, Qinglin Feng and Chunlai Ma

Department of Materials Science and Engineering, Tsinghua University, Beijing 100084, People's Republic of China. E-mail: cb_mao@263.net

Received 17th February 1999, Accepted 16th July 1999

A new process is developed to functionalize an inorganic substrate with an organic polycarboxylic chelating agent to obtain a biomimetic template for mimicking biomineralization for the synthesis of films or coatings. A titanium plate is first placed in ethylenediaminetetracetic acid (EDTA) solution to effect chemisorption and self-assembly of EDTA molecules on the plate. The plate is then aged in supersaturated hydroxyapatite [$(Ca_{10}(PO_4)_6(OH)_2$, HA] solution to mimic biomineralization. The functionalization process is found to be very effective in creating a surface with an organized arrangement of carboxylate ions ($-COO^-$) with the orientation of lone pairs of electrons on O perpendicular to or radiating from the substrate surface. The coating is formed through the plate-like outgrowth of HA grains along the [001] direction under the mediation of the functionalized surface, giving rise to the coexistence of two kinds of microstructural patterns in coating. One is a parallel arrangement of the plate-like HA grains with (001) planes preferably parallel to the substrate surface, the other is a radial arrangement of the plate-like HA grains with the [001] direction radiating from one surface core and the (111) planes preferably parallel to the surface. The mineralization mechanism is discussed on the basis of the conformation of the self-assembled EDTA molecules and the interfacial molecular recognition, analogous to the biomineralization, including electrostatic interactions, hydrogen bonding, stereochemical arrangement and geometrical correspondence.

1 Introduction

The synthesis of inorganic materials through a process mimicking biomineralization, *i.e.* biomimetic synthesis, has been regarded as a promising approach to the synthesis of low-cost inorganic materials with the desired properties.[1–4] The archetypes of the interesting process originate from biomineralization in organisms, where minerals nucleate and grow from supersaturated aqueous solution under the mediation of an organic matrix secreted by the cells.[5] There are four stages of construction resulting in the development of organized biomineralized architectures.[6,7] Stage I is supramolecular preorganization, where an organized reaction environment is built through self-assembly of an organic matrix before mineral nucleation. At the interface between the assembled organic matrix and the inorganic solution, there are functional groups ($-SO_3H$, $-OH$, $-OPO_2H$, $-NH_2$, *etc.*) to provide the organic matrix (collagen, polysaccharide, *etc.*) with a functionalized surface. Stage II is interfacial molecular recognition, where inorganic mineral nucleates from an inorganic solution at the interface under the direction of preformed organic supramolecular assemblies. The molecular recognition between mineral nuclei and organic surfaces leads to site-directed inorganic nucleation. Such recognition can be considered analogous in part to the interactions between substrates and enzyme receptor sites, antigens and antibodies. The possible mechanisms of molecular recognition involve the complementarities of lattice geometry, electrostatic potential, polarity, stereochemistry, spatial symmetry and topography.[7] Stage III is vectorial regulation, where mineral nuclei grow vectorially into crystals and the crystals are assembled into minerals. At this stage, the growth direction, orientation, texture, crystal size and shape are controlled through regulation of the organic matrix. Stage IV is a cellular process associated with a variety of constructional processes, where higher-order architectures with elaborated ultra- and micro-structural properties are built with the active participation of the cell. This stage leads to differences between biological and synthetic materials. According to the functions of the four stages, biomineralization can be mimicked with the four stages as biological archetypes.

So far, a variety of inorganic materials have been synthesized by this process, such as nanoparticles,[1] thin films,[2] coatings,[2] porous materials[3] and materials with complex forms.[4] The key point lies in the design and preparation of an organized functionalized surface. In biomineralization, an organized functionalized surface results from the preorganization of an organic matrix through a self-assembly process.[5,6] In biomimetic synthesis, the organization of functional groups can be realized either through a self-assembly process of amphiphilic surfactant (lipid, stearic acid, *etc.*) in liquid state systems such as Langmuir monolayers, microemulsions, liquid crystals and so on,[1–4,8] or through grafting or adsorption of functional groups or organic molecules on solid substrates.[2] The former process is suitable for the biomimetic synthesis of nanoparticles, porous materials and materials with complex forms.[1–4] The latter process is suitable for the biomimetic synthesis of films or coatings on solid substrates.[2]

For the biomimetic synthesis of coatings on inorganic substrates, *e.g.* phosphates on titanium as bone implants, the functionalization methods usually used include self-assembly of organic silanes[2,9] and chemical treatment by inorganic acid or base.[10,11] Recently, we tried to develop a new functionalization method where an organic chelating agent with several functional groups such as ethylenediaminetetracetic acid (EDTA, labeled as H_4Y) is strongly chemisorbed and self-assembled on the inorganic substrate with several remnant functional groups exposed. EDTA is a single hexadentate

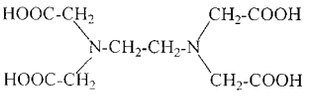

Scheme 1

chelon (Scheme 1).[12] The four oxygen atoms in four carboxyl groups (–COOH) and two nitrogen atoms all have the ability to coordinate with metal ions due to their lone pairs of electrons. The existing form of EDTA, which can be H_6Y^{2+}, H_5Y^{+}, H_4Y, H_3Y^{-}, H_2Y^{2-}, HY^{3-}, Y^{4-}, or a mixture of some of them, depends on the pH of the solution.[12] When EDTA coexists with "free" metal ions (M), a complex with stoichiometry of 1:1 (EDTA:M) will be formed.[12] When EDTA solution interacts with surface metal ions on a solid oxide substrate, adsorption of EDTA takes place as a rather rapid surface complexation process.[13–16] The adsorption of EDTA on oxides has been widely investigated owing to its important role in the chemical dissolution of metal oxides such as magnetite[17] and γ-Al_2O_3.[18] However, no results have been reported about the adsorption of EDTA on titanium with a surface oxide layer.

In recent years, self-assembled monolayers (SAMs) have been studied extensively owing to their important role in surface/interface science and technology,[19] and biomimetic materials synthesis.[20] The formation of SAMs of carboxylic acids on metals has been investigated in systems such as n-alkanoic acids on the native oxides of Al, Ag and Cu,[21,22] dicarboxylic acids on the native oxide of Al,[23] and acid derivatives containing biphenyl or naphthyl groups on the native oxides of Ag and Au.[24] However, no researchers have considered the possibility of the self-assembly of polycarboxylic acids such as EDTA molecules on the native oxide of a Ti surface and further creation of a functionalized organized surface as a template for biomimetic synthesis.

In this paper, taking the biomimetic synthesis of a biocompatible hydroxyapatite (HA) coating on titanium, which is one of the promising bone implant materials, as an example, we hope to functionalize the titanium with EDTA, to understand the chemisorption and self-assembly behaviour of EDTA molecules on the solid surface and the mechanism of biomineralization. In addition, unlike the self-assembly process of surfactants in liquid state systems[1–4] or the chemisorption of functional molecules on the surface of a single crystal substrate,[20] which can result in a homogeneous organized functionalized surface, chemisorption and self-assembly on polycrystalline inorganic substrates give rise to inhomogeneous surfaces where the functional groups form different uniform "lattices" in different domains across the whole substrate surface. Therefore, we shall also show that such inhomogeneities will result in the coexistence of several mineralized microstructural patterns. In fact, in the area of histochemical and bioinorganic chemical studies of bones and teeth, EDTA has been widely used as a demineralizing agent for separating proteins (*e.g.*, collagen, phosphoproteins), that are insoluble in the EDTA solution, from the calcified bones and teeth with preservation of the activity of cells and organic matrix by dissolution of biominerals (*e.g.*, hydroxyapatite) due to the acidity of EDTA, and its ability to chelate calcium ions.[25–33] The dissolution of HA in the bone will be promoted by the formation of complexes of Ca^{2+} and EDTA.[34] For example, Glimcher *et al.*[26,28–30] studied successfully the characteristics and roles of organic matrix (collagen) in the biomineralization of bones and teeth through the extraction of the EDTA-insoluble organic matrix from tissue as an initial step.

2 Experimental

2.1 Biomimetic mineralization

A supersaturated solution of HA ($[Ca^{2+}]=4$ mM) was prepared according to the procedure reported in ref. 8. The disodium salt of EDTA (Na_2H_2Y) was used to prepare the EDTA solution because it has a higher solubility in water than pure EDTA.[12] The EDTA solution ($[H_2Y^{2-}]=0.05$ mol l^{-1}) was controlled at pH = 4.4 to give EDTA in the solution in the form of H_2Y^{2-}.[12] A 2 mm thick titanium plate, prepared by rolling deformation, was cut into small square pieces (1 cm × 1 cm). The plates were polished metallographically with SiC emery paper to remove the oxide surface layer. The final polishing was performed with no. 800 paper and the final thickness of the polished plates was *ca.* 1 mm. The plates were ultrasonically washed in acetone for *ca.* 10 min and rinsed in deionized water for 1 min. The plates were divided into two groups. The first group was aged in water at room temperature, and are denoted AS-Ti. The second group was aged in the EDTA solution at room temperature, and are denoted EDTA-Ti. Both groups were taken out after one day and rinsed in deionized water for 1 min and then dried at 60 °C for one day. Subsequently, one plate of each group was placed separately in a 50 ml supersaturated solution of HA at room temperature for up to 2 months to induce coating formation.

2.2 Characterization

The Ti substrates after aging in EDTA solution were characterized by X-ray photoelectron spectroscopy (XPS) on an ESCALAB 220i-XL system with a Mg-Kα source. Reflection–absorption infrared (RAIR) spectra of the adsorbed EDTA layer on Ti were taken with a Nicolet Magna IR 750 spectrometer. The angle of incidence was 80° (near grazing) with p-polarized light. A gold coated wafer was used as the reference for the spectra. To avoid the effect of adsorbed water vapour on the measurements, the sample was dried at 60 °C for 1 h before IR experiments. An L116C ellipsometer was used for thickness measurements of the adsorbed EDTA layer. The He–Ne laser light was incident at 70° on the sample. A real refractive index of 1.47 was assumed in the thickness calculations.[21] The changes of pH values during the aging of Ti in the HA solution were measured *in situ* with a digital pH meter. The phase composition and orientation of the substrate and coating were determined by X-ray diffraction (XRD) on a Rigaku D/max RD diffractometer with a Cu target. To observe the morphology of the coatings by scanning electron microscopy (SEM), a knife was used to cut between the coatings and the substrate, and then the coatings were fractured to expose a fresh fractured cross section, followed by coating with gold by ion beam sputtering. The SEM images were observed using a Hitachi S-450 scanning electron microscope coupled with an energy dispersive X-ray analysis (EDAX) system.

3 Results and discussion

3.1 Surface adsorption, self-assembly and functionalization

3.1.1 Surface adsorption. The transmission infrared spectra of isotropic crystalline EDTA and its di- and tetra-sodium salts, as well as its metal chelates were investigated previously.[34–38] These can be used in comparison with the RAIR spectra to obtain useful information about the stereochemistry of the adsorbed EDTA molecules. Such a comparison is based on a surface selection rule which gives rise to a preferential excitation of vibrational modes with dipoles normal to highly reflecting metallic surfaces.[39,40] It should be stated that the surface of the titanium plates is very flat after sequential polishing with different emery papers, which is confirmed by the fact that no pits and cracks were observed on the surfaces of the plates by SEM. Such flatness makes certain the applicability of the surface selection rule of the grazing RAIR in the present experiments. The RAIR spectra for an EDTA layer on titanium are shown in Fig. 1. The low-frequency region (Fig. 1a) may contain several important features of structural significance of the monolayer assembly that are relevant to molecular orientation, interfacial chemistry and crystallinity. There are four peaks at 1500–1800 cm^{-1} which correspond to the COO stretch modes in different groups.[34–38] The strong

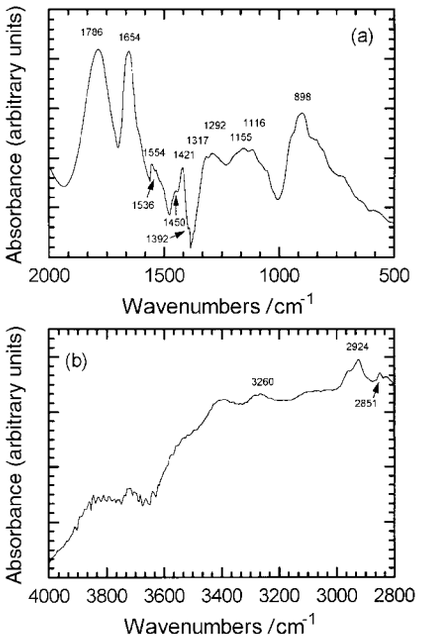

Fig. 1 Reflection–absorption IR spectra for a monolayer of EDTA on Ti. (a) Low-frequency region. (b) High-frequency region.

peak at 1786 cm^{-1} corresponds to the free carboxyl groups (–COOH). The bands at 1654 and 1554 cm^{-1} are assigned to the asymmetric stretch mode (ν_a) for carboxylate ions coordinated to surface titanium ions (–COOTi) with different coordination configurations, whereas the bands at 1536 cm^{-1} is attributed to ν_a for uncoordinated (free) carboxylate ions ($-COO^-$).[38] These assignments are based on the following demonstrated results.

(1) H_2Y^{2-} ions exist in the disodium salt of EDTA as structure A:[34]

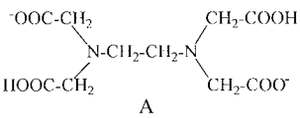

A

(2) Polycarboxylic acids such as EDTA might be chemisorbed on an oxide surface through reactions (1)–(3):[41–45]

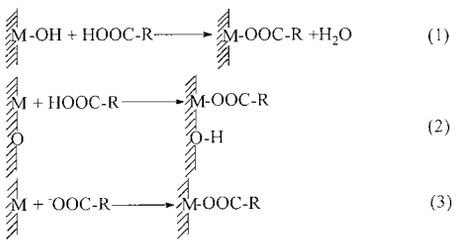

where M–OH, M, O, HOOC–R and $^-$OOC–R denote chemisorbed hydroxy on the oxide surface, the coordinatively unsaturated surface (c.u.s.) metal ions, the c.u.s. O^{2-} ions, the carboxyl groups of EDTA, and the carboxylate ions of EDTA, respectively. That is, no matter whether the surface metal ions are highly hydroxylated or not, a large number of M–OOC–R bonds may be formed to bind substrate and EDTA molecules together. The titanium substrate is always terminated with an oxide layer. Upon exposure to a water-containing environment, the surface oxide reacts rapidly with water molecules to form a hydroxylated surface through the dissociative chemisorption of water molecules.[46] Therefore, when the titanium substrate contacts an EDTA solution where the form of EDTA is H_2Y^{2-}, EDTA will be chemisorbed onto the titanium through reactions (1), (2) or (3).

(3) The frequencies of the COO asymmetrical vibrational modes decrease in the sequence: –COOH groups, coordinated carboxylate ions and uncoordinated carboxylate ions.[38]

The frequencies of the symmetric vibrational modes (ν_s) of coordinated or uncoordinated carboxylate ions are usually between 1300 cm^{-1} and 1500 cm^{-1}.[38,47] Since there are two ν_a bands for –COOTi groups with different coordination modes and one ν_a band for $-COO^-$ ions, there should have been three corresponding ν_s bands. It has been demonstrated that the difference between ν_a and ν_s (denoted Δ) is different for coordinated and uncoordinated carboxylate ions.[38] For $-COO^-$ ions, the Δ value is *ca.* 144 cm^{-1}, whereas it varies between 50 and 300 cm^{-1} for coordinated carboxylate ions depending on the coordination modes.[38] According to this result, the ν_s corresponding to $-COO^-$ with ν_a at 1536 cm^{-1} will be *ca.* 1392 cm^{-1}. Indeed, there is a shoulder band at *ca.* 1392 cm^{-1} in Fig. 1a, which is much weaker due to the surface selection effect inherent in RAIR,[21,22,24,40] *i.e.*, the dipole of the ν_s mode for free COO^- ions is at such a large angle with respect to the surface normal that the projection component of the ν_s mode along the surface normal is much shorter than that of the ν_a mode. In the transmission IR spectrum of the disodium salt of EDTA, the intensities of ν_a and ν_s do not differ so much.[34–38] A carboxylate ion can coordinate to a metal ion in various configurations, from bridging bidentate (B), chelating (C) to unidentate ligand (D).[38]

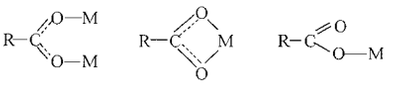

B C D

The two bands at 1450 cm^{-1} and 1421 cm^{-1} may thus correspond to ν_s modes of two kinds of –COOTi groups with different configurations. Table 1 lists the assignments of the IR bands in the low-frequency region and the frequencies for the corresponding bands reported in the literature.[22,38,48–50] The configurations of the –COOTi groups will be discussed in Section 3.1.2. The existence of IR bands for C–O, CH_2, C–N, and C–H groups confirms the chemisorption of EDTA on Ti and the correct IR band assignments of carboxyl groups and carboxylate ions.

In the high-frequency region as shown in Fig. 1b, the O–H stretching band for the –COOH group is seen at *ca.* 3300 cm^{-1},[38] which indicates that there are unionized –COOH groups in the adsorbed EDTA molecules and thereby confirms the correct assignment of ν(COOH) at 1786 cm^{-1}. The two bands at 2924 and 2851 cm^{-1} can be attributed to the asymmetric and symmetric methylene vibrations, $\nu_a(CH_2)$ and $\nu_s(CH_2)$, respectively.[48] While the CH_2 groups are the most abundant of all the groups in an adsorbed EDTA molecule, the intensities of $\nu_a(CH_2)$ and $\nu_s(CH_2)$ are however lower than those of ν_a(COOTi) and ν(COOH). This is due to the surface selection effect,[21,22,24,39,40] *i.e.* the orientations of the six CH_2 groups in one adsorbed EDTA molecular are not identical and some of them are oriented so that the projection components along the surface normal for both symmetric and asymmetric stretching vibrations are nearly zero since the dipoles for $\nu_a(CH_2)$ and $\nu_s(CH_2)$ are perpendicular to each other.

The average ellipsometric thickness for the adsorbed EDTA layer is *ca.* 0.74 nm through averaging over seven spots for a given sample. This suggests a high coverage of the EDTA molecular layer on the titanium substrate. In addition, the fact that the grazing incidence RAIR experiment can be conducted at all on such an adsorbed layer also confirms the high coverage.

Fig. 2 depicts the XPS spectra of Ti 2p, O 1s, and C 1s of the EDTA-treated titanium surface after rinsing and drying.

Table 1 IR vibration modes assignment for an EDTA layer on titanium

Mode description[a]	Frequency in RAIR spectrum/cm^{-1}	Peak intensity in RAIR spectrum	Reported frequency/cm^{-1}	Reference
ν(C=O, in COOH)	1786	Very strong	1750	38
ν_a(COO in COOTi (I))[b]	1654	Strong	1604	38
ν_s(COO in COOTi (I))	1450	Medium	1376	38
ν_a(COO in COOTi (II))[c]	1554	Medium	1526	38
ν_s(COO in COOTi (II))	1421	Medium	1449	38
ν_a(COO$^-$, uncoordinated)	1536	Medium	1560	38
ν_s(COO$^-$, uncoordinated)	1392	Weak	1416	38
ρ_w(CH$_2$) or ν(C–O)	1317	Medium	1333 or 1374	48,49
ρ_t(CH$_2$)	1292	Medium	1288	22
δ(C–H)	1155	Medium	1188	50
ν(C–N)	1116	Medium	1116	35
ρ_r(CH$_2$) or π(CH)	898	Medium	912 or 855	38,48

[a]ν, stretch; ν_a, antisymmetric stretch; ν_s, symmetric stretch; ρ_w, wagging; ρ_t, twisting; δ, deformation; ρ_r, in-plane rocking; π, out-of-plane bending. [b]COOTi (I), unidentate configuration. [c]COOTi (II), bidentate chelating configuration.

Curve-fitting of the Ti 2p spectrum (Fig. 2a) revealed that the spectrum can be resolved into two peaks centred at 463.89 and 458.27 eV, corresponding to Ti 2p$_{1/2}$ and Ti 2p$_{3/2}$ in TiO_2, respectively.[51,52] It is thus evident that the surface oxide layer of EDTA–Ti is TiO_2. Many researchers also found that TiO_2 is the natural oxide layer on titanium at room temperature.[52–54] Since the thermodynamically stable form of TiO_2 at low temperature is anatase (tetragonal, $a=0.3783$ nm, $c=0.951$ nm, JCPDS 4-477),[55] the surface oxide layer can be regarded as the anatase form[56] although rutile and anatase are not differentiated by XPS. Curve-fitting of the O 1s spectrum (Fig. 2b) showed three peaks with binding energies of 532.99, 531.49, and 529.74 eV, which correspond to O 1s electrons in –COOH groups and carboxylate ions (–COO$^-$) in chemisorbed EDTA,[51,57] hydroxy in –COOH groups, chemisorbed hydroxy groups and physisorbed H_2O,[51] and the oxide lattice of the surface anatase layer,[51,52] respectively. The C 1s spectrum (Fig. 2c) can be resolved into four peaks with binding energies of 288.2, 286.24, 284.61, and 280.61 eV, corresponding to carbon in –COOH groups and –COO$^-$ ions of chemisorbed EDTA, –CH$_2$– groups of chemisorbed EDTA, contamination impurities inherent to the XPS spectrometer, and carbide impurities introduced through the polishing by SiC emery paper, respectively.[51,57] The XPS results confirm the chemisorption of EDTA on the surface anatase layer.

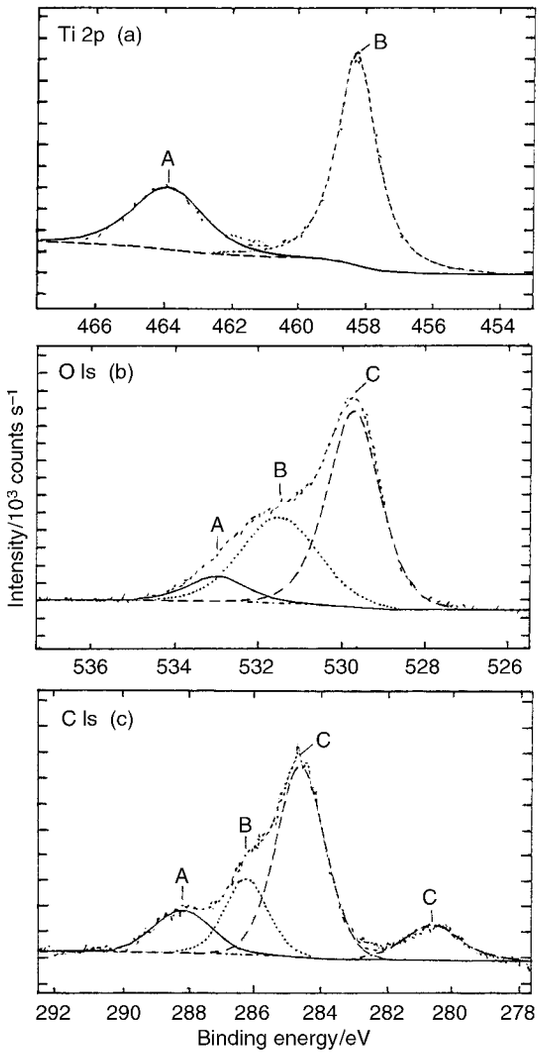

Fig. 2 XPS spectra of Ti 2p, O 1s and C 1s for an EDTA-treated titanium plate.

3.1.2 Self-assembly of EDTA molecules and configurations of self-assembled EDTA molecules. To discuss the adsorption mode of EDTA on an anatase surface layer, one should first take into account the surface chemistry of anatase, which has been extensively investigated.[55] There are three types of c.u.s. Ti^{4+} ions on anatase, as schematically illustrated in Fig. 3.[55] One is the four-coordinated Ti^{4+} ions on faces (11*l*) such as 110, 111 and 113 as well as at the edge of the 110 face. The second is the five-coordinated Ti^{4+} ions which participate in Lewis acid–base pairs (c.u.s.Ti^{4+}–c.u.s.O^{2-}) on the most characteristic faces such as $101 \equiv 011$ and $100 \equiv 010$. The third is the five-coordinated Ti^{4+} ions participating in Lewis

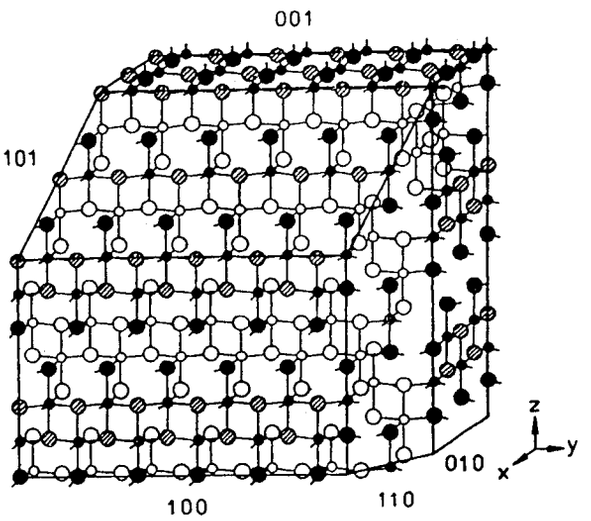

Fig. 3 Schematic illustration of the surface lattices of different exposed planes of anatase (reprinted from ref. 55). •, c.u.s. Ti^{4+} ions; ○, saturated Ti^{4+} ions from the subsurface layers; ●, c.u.s. O^{2-} ions; ○, saturated O^{2-} ions from the surface layers; ▨, saturated O^{2-} ions from the subsurface layers. Notice that the dangling bonds for c.u.s. ions are also shown.

acid–base rows of c.u.s.Ti^{4+}–c.u.s.O^{2-}–c.u.s.Ti^{4+}–c.u.s.O^{2-}⋯ on faces such as 001 and 112 and at the edges 101×111. Ti^{4+} ions from isolated acid–base pairs are more electrophilic and thereby more acidic than those from acid–base rows in that the electrophility decreases due to the formation of stronger bonds with two not one c.u.s. O^{2-} ion.[55] The most appropriate centres for dissociative adsorption are situated on face 110 because face 110 contains the most acidic four-coordinated Ti^{4+} ions, and two c.u.s. O^{2-} ions act as a Lewis base.[55] One can imagine that a self-assembly process may take place after the chemisorption of EDTA, just like the self-assembling of alkanethiolates on gold, fatty acids on oxides, and organic silanes on oxides.[19,58] A self-assembled monolayer (SAM) will be formed, *i.e.* organization of complex, semiflexible organic molecules within a quasi-two-dimensional assembly, resulting from a delicate interplay between substrate–adsorbate interactions, non-bonded interactions between adsorbates—electrostatic and van der Waals (VDW) forces—and intramolecular interactions such as bond stretches, angle bends, and torsions.[19] The self-assembly process can be driven by the non-covalent interaction between and within chemisorbed EDTA molecules, such as electrostatic repulsion and VDW forces.[58]

Tao[21] investigated self-assembled monolayers of n-alkanoic acids ($CH_3(CH_2)_mCOOH$) on the native oxide surfaces of Ag, Cu and Al. He found that the structure of the adsorbed film was strongly dependent on the underlying metal structure and the metal substrate dominated the binding geometry of the carboxylate head group and the packing density. The n-alkanoic acids dissociated completely on all of these metals and formed a carboxylate overlayer. The two oxygen atoms of the $-COO^-$ bound to the Ag surface (AgO) nearly symmetrically, while the carboxylate bound to the Al and Cu surface (Al_2O_3 and Cu_2O) asymmetrically. He considered that such differences resulted from the different surface lattices of the metal oxides and different binding strengths of carboxylate on each metal. In the present study, EDTA is a polycarboxylic acid. RAIR and XPS results have demonstrated that the chemisorbed EDTA molecules contain undissociated –COOH, uncoordinated $-COO^-$ and coordinated $-COO^-$ (–COOTi), *i.e.* not all of the two carboxylic groups in H_2Y^{2-} dissociate and bind to the native oxide on Ti, possibly due to the strong acidity of the EDTA solution and steric limitations on the surface.

Based on the surface selection rule for grazing RAIR, the following structural characteristics for the adsorbed EDTA layer can be drawn from the RAIR results as shown in Fig. 1.[21,22,24,39,40]

(1) The intensities of the stretching mode of the carbonyl group in –COOH (1786 cm^{-1}) is very high, suggesting that the carbonyl group in –COOH has a significant component along the surface normal, and is most probably parallel to the surface normal.

(2) The absorption band of the symmetric vibration mode for uncoordinated $-COO^-$ ions is very weak and overlapped with the 1421 cm^{-1} band for ν_s(COOTi) with respect to the stronger asymmetric vibration mode (1536 cm^{-1}), indicating that $-COO^-$ ions are exposed so that the transition dipoles of symmetric vibration modes have a much smaller component along the surface normal than those of asymmetric vibrational modes.

(3) There are two kinds of COOTi groups with ν_a at 1654 and 1554 cm^{-1}. On the other hand, there are two kinds of c.u.s. Ti^{4+} ions, *i.e.* four-coordinated [*e.g.* on (110)] and five-coordinated [*e.g.* on (100)], and the basicity of the former is weaker than the latter.[55] Tao[21] found that the peak frequency for symmetric carboxylate shifts to a higher value, reflecting the higher coordination strength, when carboxylate is bound to surface cations with stronger basicity. Moreover, the Δ value for –COOTi with a unidentate configuration is usually higher than the value for that with a bidentate chelating configuration.[38] Therefore, the 1654 and 1450 cm^{-1} bands should be assigned as ν_a and ν_s for carboxylate bound to the five-coordinated c.u.s. Ti^{4+} ions with a unidentate configuration and a Δ value of 204 cm^{-1} [COOTi(I)], whereas the bands at 1554 and 1421 cm^{-1} correspond to ν_a and ν_s for carboxylate bound to the four-coordinated c.u.s. Ti^{4+} ions with a bidentate chelating configuration and a Δ value of 133 cm^{-1} [COOTi(II)].

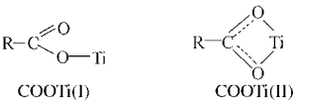

COOTi(I) COOTi(II)

(4) The substantial intensity of the ν_a mode with respect to the low intensity of the ν_s mode for COOTi(I) indicates that the carboxylate groups bind to the surface at an angle so that the transition dipoles of the ν_a mode are at a smaller angle to the surface normal than those of ν_s, *i.e.* the transition dipoles of the ν_a mode have a much larger component along the surface normal.

(5) The presence of both ν_a and ν_s peaks for COOTi(II) with nearly identical intensities shows that the carboxylate head group should bind to the surface in such an orientation that the transition dipoles of the ν_a and ν_s modes are at a nearly identical angle to the surface normal (*i.e.*, close to 45°), resulting in nearly identical projection components along the surface normal.

It should be pointed out that an accurate comparison of the intensities for IR absorption bands should be based on the integrated intensities, *i.e.* the area of a band. Since the ν_a and ν_s bands for different carboxylate groups overlap with each other and only their peak tips can be clearly identified, the above comparison of the intensities is qualitative. However, it is good enough to provide information on the stereochemical characteristics of the adsorbed molecules.

In the XPS C 1s spectrum, the peak at 288.20 eV corresponds exactly to the carboxylate ions (*e.g.* 288.20 eV for CH_3C^*OONa).[51] The peak corresponding to C 1s of –COOH should be close to 289.30 eV (*e.g.* 289.30 eV for CH_3C^*OOH). Therefore, it may be overlapped by the former. This result indicates that the surface concentration of –COOH groups is low, although it shows a very strong absorption band at 1786 cm^{-1} due to the surface selective excitation effect in RAIR.[39,40] Furthermore, during chemisorption and self-assembly of EDTA on Ti, there might be a cooperativity, *i.e.* geometry matching, between the separation of the two Ti–OOC bonds and that of two c.u.s. Ti^{4+} ions with which two separate $-COO^-$ groups of one EDTA molecule are bonded. The distance between the two Ti–OOC bonds in one chemisorbed EDTA molecule is determined, therefore, by the surface Ti^{4+} sublattice. Moreover, the stereochemical conformations of the three main component parts should be maintained during self-assembly, and should thereby be considered to describe the conformation of self-assembled EDTA molecules. One component is the planar triangular conformation of resonance stabilized carboxylate ions where the negative charge and π electrons are delocalized through resonance and are spread equally over the two oxygen atoms. In addition, lone pairs of electrons exist at the oxygen with directional character that are not directly involved in chemical bonds.[59] The second is the pyramidal conformation of the tertiary amine group.[59] The third is the tetrahedral conformation of the methylene group ($-CH_2-$).[59]

From these considerations and the possible chemisorption reactions (1)–(3) as well as the RAIR, XPS and ellipsometric measurement results, we consider that two typical adsorption modes such as in Schemes 2 and 3 might be produced to reach the thermodynamically stable configuration of c.u.s. Ti^{4+} ion, *i.e.* the six-coordination nature of the Ti^{4+} ion. Schemes 2 and 3 apply to the $(h0l) \equiv (0hl)$ faces with five-coordinated c.u.s. Ti^{4+} ions, *e.g.* (100), and (11*l*) faces with four-coordinated c.u.s. Ti^{4+} ions, *e.g.* (110), respectively. Schemes 2 and 3

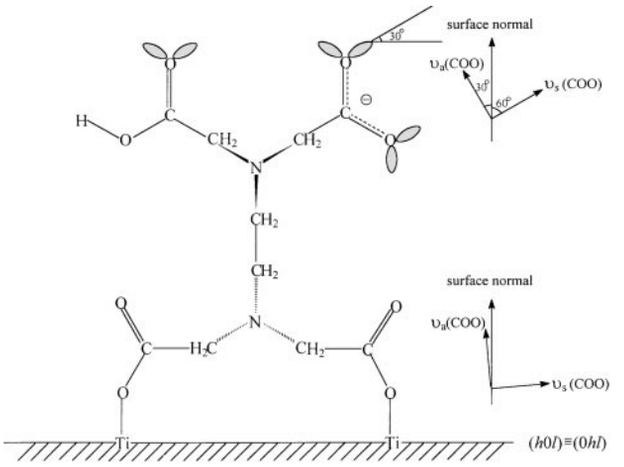

Scheme 2

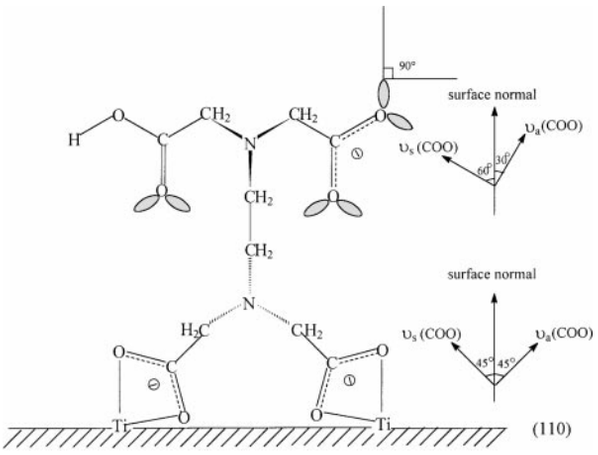

Scheme 3

represent the most likely adsorption modes of EDTA on the anatase surface. The –COOTi bonds in Schemes 2 and 3 correspond to COOTi(I) and COOTi(II), respectively.

The C–N, C–C and C–O bond lengths equal 0.1472, 0.1541 and 0.1233 nm, respectively.[60] From these data and the steric geometrical relationships, one can calculate through the planar projection on the plane of the diagram that the thickness values of the monolayer as in Schemes 2 and 3 are *ca.* 0.75 and 0.76 nm, respectively, consistent with the ellipsometric thickness (0.74 nm). Therefore, it is confirmed that a SAM of EDTA has been formed on the native oxide surface of Ti. Moreover, the bottom plane of the pyramidal geometry of the tertiary amine group is on the plane of the diagram. Thus, the length of the projection of the C–N bond on the plane of the diagram equals 0.1383 nm.[38] Using the geometry of the planar projection of Scheme 2, the interdistance between two COOTi(I) bonds, through which one EDTA molecular is anchored on the surface anatase layer, is *ca.* 0.72 nm. This separation is approximately equal to two times the lattice constant *a* (0.3783 nm) of anatase, *i.e.* two times the basic periodicity of c.u.s. Ti^{4+} ions on $(h0l)\equiv(0hl)$ planes along the $[010]\equiv[100]$ direction. For Scheme 3, the separation for two –COOTi(II) bonds is calculated to be *ca.* 0.50 nm, very close to the length of the basic repeating unit of c.u.s. Ti^{4+} ions on (110) planes along the [110] direction ($2^{1/2}a_{\mathrm{anatase}}$, *i.e.* 0.54 nm). These calculations support the hypothesis of Schemes 2 and 3. It should be stated that a slight relative rotation around the substrate normal can be made between the triangle of the carboxylate ions and the pyramid of the tertiary amine groups to maintain the tetrahedral conformation of the $–CH_2–$ group. The direction of the lone pairs of electrons on the oxygens of the carboxylate ion[61] and the relative geometrical relationship between the directions of the asymmetric and symmetric vibrational dipoles for the carboxylate and the surface normal[21,24] are also shown in Schemes 2 and 3. The orientations of the electron cloud of lone electron pairs on the oxygen atoms of carboxylate and the angle between the vibrational dipole for the carboxylate and surface normal are different between and within the schemes.

In Scheme 2 the orientation of COOTi is idealized to let the RAIR intensity of the symmetric stretching vibration of COO become zero and should have been rotated by a small angle, as illustrated by the orientation relationship between ν_a and ν_s, because its real intensity is very weak (but not zero) with respect to that of asymmetric stretching vibration, as shown in Fig. 1. Because the Ti substrate is (0001) textured, as will be shown by the XRD in Fig. 5 (later), the exposed planes of the surface anatase phase grown on such a substrate at room temperature might be limited to only a few types such as (110) and (100).[62] Since the EDTA self-assembly will be determined

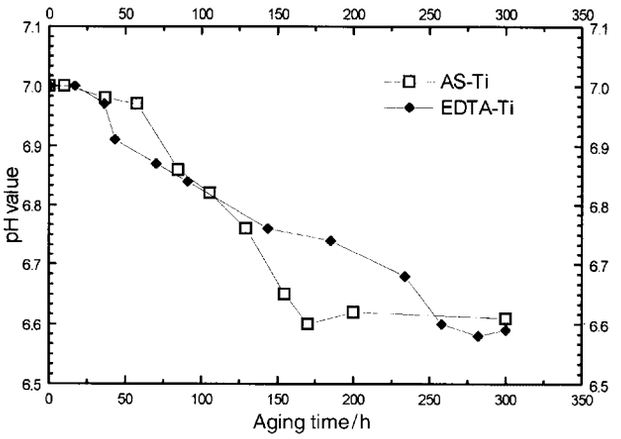

Fig. 4 Time dependences of pH values in HA solutions containing AS-Ti and EDTA-Ti.

partly by the surface lattice of the exposed planes where EDTA molecules are situated and the polycrystalline surface anatase layer, the surface state will be a mixture of adsorption configurations with different stereochemistry such as Schemes 2 and 3. Walczac *et al.*[63] also found that a SAM was made up of mixed domains with different stereochemical orientations, consistent with our considerations.

3.2 Biomimetic mineralization on an EDTA functionalized substrate

3.2.1 Biomimetic mineralization. Precipitates appear on the beaker wall and in the bulk solution for the HA solution containing AS-Ti after *ca.* 2 days. No continuous and uniform coatings are formed on AS-Ti except island-like white spots which might have been picked up from the bulk solution. The fact that the majority of the white spots can be washed away confirms that the white spots are formed from precipitates appearing from the bulk solution. For the HA solution containing EDTA-Ti, however, no precipitates appear in the bulk whereas a layer of uniform and continuous coating is formed on the titanium substrate. Crystallization of HA can be written in terms of eqn. (4):

$$10Ca^{2+} + 6PO_4^{3-} + 2OH^- \rightarrow Ca_{10}(PO_4)_6(OH)_2 \qquad (4)$$

Therefore, the pH reduction is a signal of HA crystallization on titanium or in the bulk solution. Fig. 4 depicts the time dependences of the pH values of the AS-Ti and EDTA-Ti solutions. For the EDTA-Ti solution, the pH value decreases after *ca.* one day due to crystallization on the EDTA-Ti until aging for *ca.* 10 days, and levels off at *ca.* 6.6. For AS-Ti, the

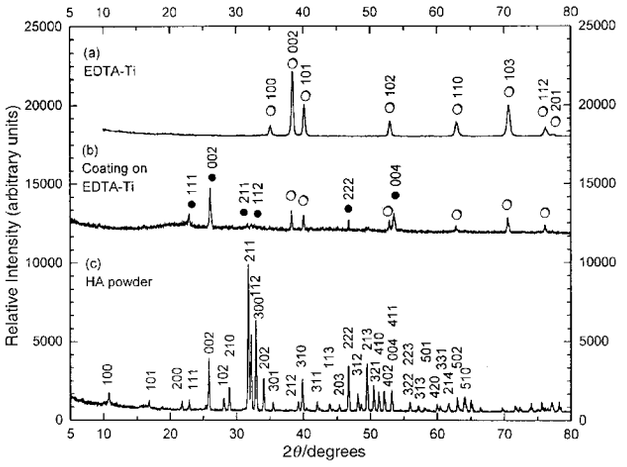

Fig. 5 XRD patterns of EDTA-Ti before (a) and after (b) coating formation, and HA powder (c). Note that all the peaks in (c) are the diffraction lines for HA. (○), Ti; (●), HA.

pH value decreases after 60 h more rapidly due to the precipitation in bulk solution, and also levels off at *ca.* 6.6 after 170 h.

Fig. 5 depicts the XRD patterns of surface EDTA-Ti before and after coating formation as well as that of the randomly oriented HA powder. It is revealed that the coating consists of nearly pure HA phase (hexagonal, $a=0.9418$ nm, $c=0.6884$ nm, JCPDS 9-432) within the detection limits of XRD. The titanium shows an (001) preferred orientation, which results from rolling deformation.[64] Through careful comparison of the XRD patterns of the HA coating and HA powder, only some of the peaks expected for HA plus those for Ti exist in the diffraction pattern of the coating, *i.e.* (00*l*) type, (*lll*) type, (211) and (112), while all the diffraction lines appear for randomly oriented HA powder. In addition, the intensities of the (00*l*) and (*lll*) diffraction lines normalized to that of the (211) line (the strongest one for randomly oriented HA powder) of the HA in the coating are much higher than those in the HA powder. Therefore, the HA coating is in a highly preferred orientation with (00*l*) and (*lll*) planes parallel to the substrate surface.

Fig. 6 displays typical SEM micrographs of the HA coating on titanium after aging for 300 h. The coating is uniform and composed of plate-like grains which grow out from the titanium surface, suggesting that the heterogeneous nucleation occurred on the functionalized titanium at the substrate/solution interface. EDAX analysis showed that the Ca/P molar ratio is 1.587, very close to the stoichiometric value (1.67) for HA. Moreover, two types of grain arrangements can be observed. One is the parallel arrangement (Fig. 6b), *i.e.* the plate-like grains are parallel to each other along their long axes; the other is the radial arrangement (Fig. 6c), where the plate-like grains radiate from a central core on the substrate along their long axis to form an upward floret-shaped cone. On the SEM images, the long axis of the plate-like grains in the radial pattern that constitute the cone shape is at an angle of *ca.* 35° with the substrate plane (Fig. 6a and c). Previous studies have shown that HA grains always tend to grow along the [001] direction, which results in a plate habit, and the long axes of the plate-like grains are parallel to the crystallographic [001] direction.[65] Thus, one can infer the type of preferred orientation from the grain arrangements shown in the SEM images. Obviously, the parallel arrangement in Fig. 6 corresponds to a (001) preferred orientation, as schematically illustrated in Fig. 7a. From the crystal structure of HA, the angle between the (001) and (111) planes, and that between the [001] direction and the (111) plane, can be calculated to be 55.6° and 33.4°, respectively, consistent with the angles measured in

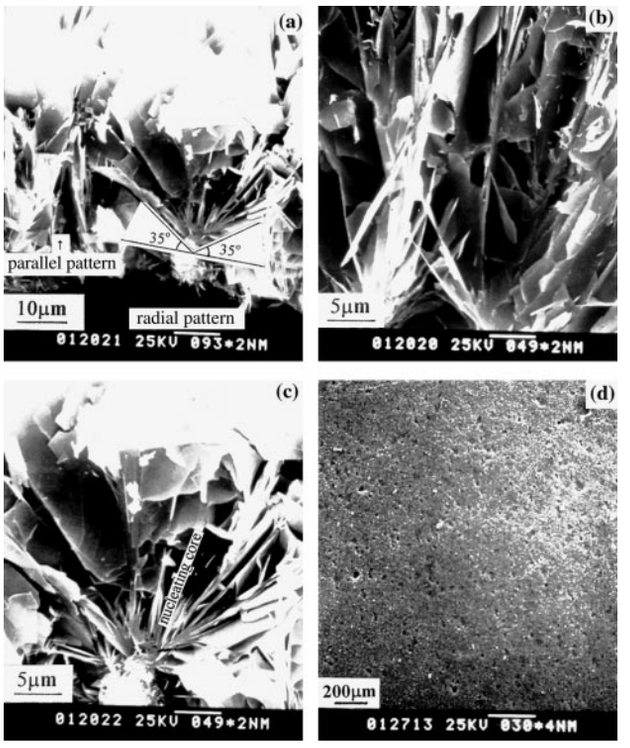

Fig. 6 SEM micrographs of HA coating on EDTA-Ti, (a) typical morphology of cross-section; (b) parallel microstructural pattern in (a) in higher magnification; (c) radial microstructural pattern in (a) in higher magnification; (d) top-view morphology of the coating. Notice that the angle between the long axis of the plate-like grains in the radial pattern and the substrate plane, and the nucleating surface core are denoted.

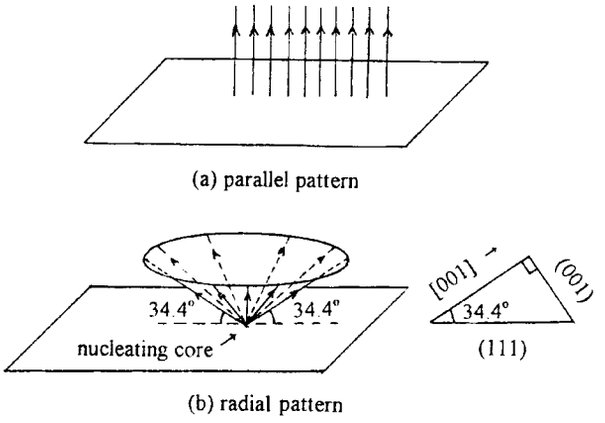

Fig. 7 Schematic illustration of two types of plate-like grain arrangements. (a) Parallel pattern; (b) radial pattern. The arrows denote the [001] directions of HA grains.

the SEM image which is a projection perpendicular to the cross-section (Fig. 6c). Hence, the radial arrangement corresponds to (111) texture with plate-like grains radiating along the [001] direction, as illustrated in Fig. 7b. Therefore, the two components of texture determined by XRD (Fig. 5), (001) and (111), result from the parallel and radial arrangements of the plate-like HA grains, respectively. The island-like surface of AS-Ti after aging in HA solution makes it difficult to characterize by XRD. Therefore, SEM and *in situ* EDAX together form an alternative way of characterizing AS-Ti. Fig. 8 depicts the top-view SEM morphologies of island-like precipitates on AS-Ti after aging for 300 h. The EDAX analysis suggests that the Ca/P molar ratio of the islands is 1.535, similar to the results for EDTA-Ti, indicating that the

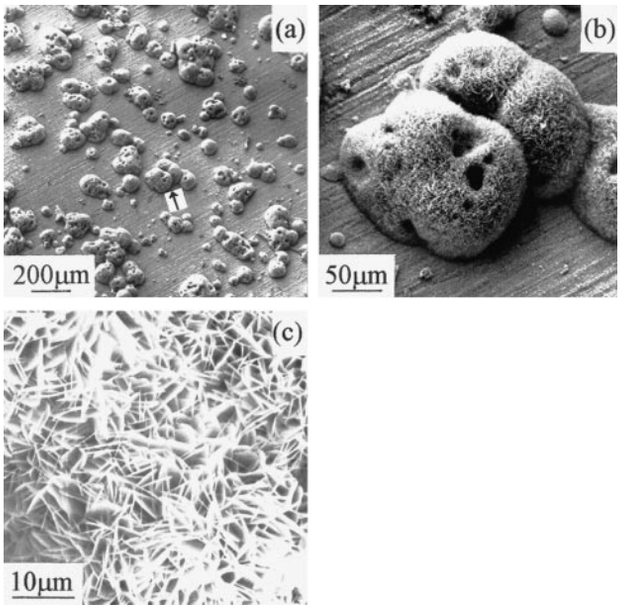

Fig. 8 Top-view SEM morphologies of island-like precipitates on AS-Ti after aging for 300 h. (a) Whole morphology. (b) Three adjacent islands (denoted with arrow in (a)) at higher magnification. (c) One island as shown in (b) at much higher magnification.

precipitates consist of HA crystals. The islands are ball-like in shape and consist of plate-like crystals. Their size varies between 50 and 150 μm. Since it is difficult to make a fractured cross-section of one island, the length of the grains can not be determined. However, analogous to the grains on EDTA-Ti, the length of the plate-like grains may be *ca.* 30 μm. Most ball-like islands are much thicker than the coating on EDTA-Ti, *i.e.* the height of an island does not equal the length of the crystal, and there are several crystals along the normal direction. This may be because the crystals can only grow on previously formed crystals if they are not favoured to form on the bare titanium substrate.

3.2.2 Mechanism of biomimetic mineralization. One of the most striking results is that the mineralized coating is made up of two types of microstructural patterns, *i.e.* parallel and radial patterns, as shown in Fig. 5 and 6. Analogous to the biomineralized microstructure, the microstructural patterns might also result from the mediation of mineral formation by an organized template through which a site-directed and directional interaction between the organic matrix and inorganic species takes place.[5–7] It is just the EDTA-functionalized titanium surface that acts as an organized template responsible for the formation of the observed interesting microstructural patterns. Since the interaction between the functionalized surface and the HA solution is site-directed and directional, it should be discussed on the basis of the detailed configuration of Schemes 2 and 3, *i.e.* the structural stereochemistry of adsorbed EDTA.

Since the EDTA-functionalized titanium plates are incubated in the HA solution with an initial pH value of 7.0, the –COOH groups, as shown in Schemes 2 and 3, will further dissociate and reach an orientation the same as uncoordinated $–COO^-$ ions after such plates are put into the HA solution. After the dissociation rapidly reaches an equilibrium between surface EDTA and the HA solution, the remnant concentration of surface –COOH will be very low. Therefore, the role of –COOH in the mediation of mineralization will be considered the same as that of uncoordinated $–COO^-$ ions. Based on the deduced conformation of the self-assembled EDTA molecules as in Schemes 2 and 3, the mechanism of HA mineralization on the titanium plate can be explored. The complex microstructure in the mineralized coating results from the controlled nucleation of HA crystals by the self-assembled EDTA surface layer through interfacial molecular recognition. Such recognition might originate from at least four aspects.

(1) Electrostatic interactions. The negatively charged $–COO^-$ ions on the surface can attract the positively charged Ca^{2+} in the solution, which promotes further complexation with PO_4^{3-} and OH^- and thereby satisfies the nucleation of HA.[66]

(2) Hydrogen bonding interactions. The OH^- ions from the solution can be adsorbed on the substrate through hydrogen bonding with O in $–COO^-$, *i.e.*, $–COO\cdots H–O$, which will favor the formation of an OH^- sublattice for HA nucleation. The formation of hydrogen bonds is a result of a specific interaction that requires the contact between "specific" sites of the partners: the "proton donor site" OH and the "proton receptor" site, the lone pair of electrons on O of $–COO^-$ ions.[61]

(3) Stereochemical arrangement. The hydrogen bond is characteristic of both stoichiometry and directionality.[61] It is stoichiometric because the number of hydrogen bonds that O in $–COO^-$ ion can form is determined by the number of lone pairs of electrons. The directional character of the hydrogen bond is a result of the directionality of the unshared electron pairs. For resonance-stabilized $–COO^-$ ions, the two lone pairs of electrons form an angle of *ca.* 60° with the C=O direction. As a consequence, a hydrogen bond with OH^- will try to adopt a structure where the OH^- direction forms an angle of *ca.* 60° with the C=O direction,[61] as shown in Scheme 4. The hydrogen-bonded OH^- ($O\cdots H–O$) can adjust its orientation to reach an angle of *ca.* 60° with respect to C=O directions, the most stable configuration of hydrogen bond.[59] Therefore, the O–H direction in the HA nuclei will be determined by the direction of lone electron pairs on O of $–COO^-$ ions. On the other hand, the arrangement of OH^- ions surrounded by a Ca^{2+} triangle along the *c* axis is characteristic of the HA structure.[67,68] Then, if the direction of the O–H bond in the OH^- ions is determined, the *c* axis of an HA nucleus constructed from these OH^- ions will be fixed, consequently resulting in the oriented nucleation. Furthermore, the HA crystals tend to grow along the [001] direction, the fastest growth direction for HA, resulting in plate-like morphology.[59,67] Hence, the functionalization mode such as in Scheme 2 will produce a surface area with an arrangement of unshared electron pairs on O of surface $–COO^-$ ions radiating from one surface core with an angle of *ca.* 30° with the substrate plane, which leads to the formation of nuclei with [001] directions radiating at an angle of *ca.* 30° with the substrate plane and subsequent radiating growth along the [001] direction as shown in Fig. 9a, and ultimately results in the formation of the radial microstructural pattern (Fig. 7b). Moreover, from Fig. 9a, one can deduce that the long axis of the plate-like HA grains (*i.e.*, the *c*-axis), will tend to be at an angle of *ca.* 30° with the substrate surface, consistent with the observed radiating angle of *ca.* 35° in the radial pattern (Fig. 6). A functionalization mode such as in Scheme 3 will create a surface area with an arrangement along the surface normal of unshared electron pairs on O of surface $–COO^-$ ions parallel to the substrate normal, which results in the oriented nucleation and subsequent oriented growth with the (001) plane preferably parallel to the substrate surface, as shown in Fig. 9b, and ultimately gives rise to the formation of the parallel microstructural pattern (Fig. 7a). It can thus be concluded that the

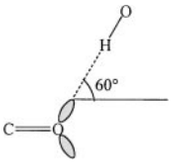

Scheme 4

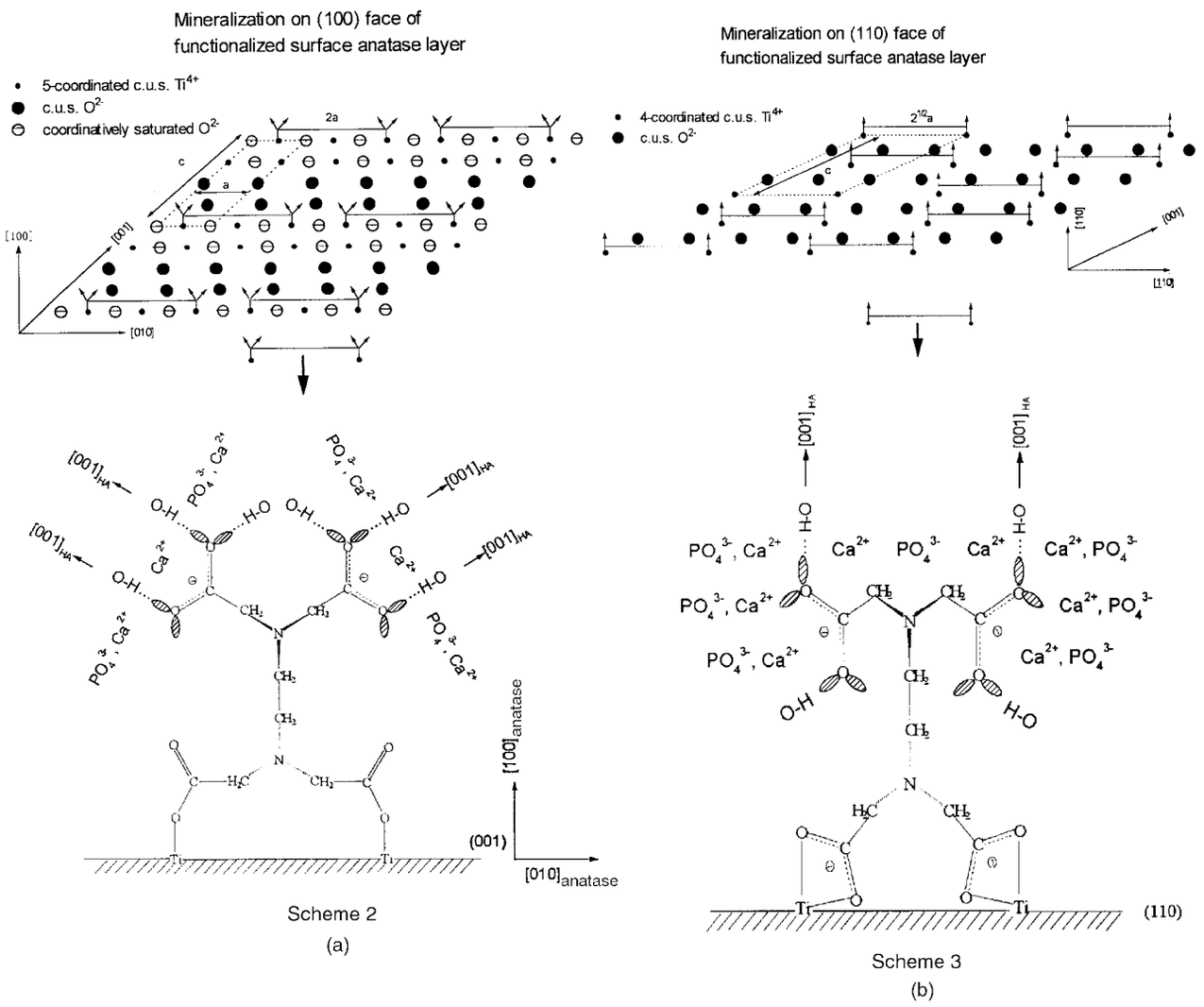

Fig. 9 Schematic illustration of the formation mechanisms of (a) radial and (b) parallel microstructural patterns, taking (100) and (110) faces of surface anatase layer as examples, respectively.

radial and parallel microstructural patterns originate from the hydrogen bonding interaction between OH^- and $-COO^-$ ions which show radial (like Scheme 2) or parallel (like Scheme 3) stereochemistry of lone pairs of electrons, as illustrated schematically in Fig. 9.

(4) Geometrical matching. The separation along [001] between the two rows of self-assembled EDTA molecules which are situated on face $100 \equiv 010$ along $[010] \equiv [100]$ or on face 110 along [1̄10] with the configuration, such as in Schemes 2 or 3, respectively, equals the lattice constant c of anatase (0.951 nm), and therefore is very close to the lattice constant a of the HA nuclei (0.9418 nm). Therefore, on the surface with a configuration like Schemes 2 or 3, the matching of distance between the two rows of $-COO^-$ ions along [001] of anatase and that between two coplanar OH^- ions, or two coplanar Ca^{2+} ions on the (001) plane of HA, might facilitate the oriented nucleation of the (001) plane of HA together with the mediation of OH^- orientation in HA by stereochemical arrangement, as discussed in aspect (3) above (Fig. 9). This may be another main reason for the formation of radial and parallel patterns. It is possible that the radial and parallel patterns might be favoured to form on the $(h00) \equiv (0h0)$ face and on the (110) face, respectively, because there is a periodicity of 0.9468 nm on the ($hk0$) planes of anatase, *i.e.* the lattice constant c of anatase is very close to the periodicity on the (001) plane of HA.

The existence of both (111) and (001) texture of the HA coating revealed by the XRD patterns of the HA coating on EDTA-Ti confirms the possibility of a geometrical match between the EDTA functionalized titanium surface and HA in light of the RAIR results. For the mineralization on EDTA molecules on EDTA-Ti with the configuration of Scheme 2, as shown in Fig. 9a, the direction of O–H groups attracted to the surface due to the hydrogen bonding is controlled to be at a radial angle of 30° with the substrate surface, and the distance of such O–H groups recognized by the two rows of EDTA molecules along $[001]_{anatase}$ is nearly equal to the lattice constant a of HA. Therefore, HA will be nucleated with $(001)_{HA}$ at an angle of about 60° to the substrate surface, which will facilitate the formation of a radial pattern with (111) texture. For the mineralization on EDTA molecules with the configuration of Scheme 3, as shown in Fig. 9b, the direction of O–H groups attracted to the surface due to hydrogen bonding is controlled to be perpendicular to the substrate surface, and the distance of such groups recognized by two rows of EDTA molecules along $[001]_{anatase}$ is nearly equal to the lattice constant a of HA. Therefore, HA will nucleate with $(001)_{HA}$ parallel to the substrate surface, resulting in the formation of a parallel pattern with (001) texture.

4 Conclusion

EDTA can be used to functionalize a naturally oxidized titanium substrate to obtain a surface with an organized arrangement of carboxylate ions, which can mimic the preorganized organic matrix in biomineralization systems.

EDTA molecules may have the ability to self-assemble into functional arrays with two $-COO^-$ groups bonding on two coordinatively unsaturated Ti^{4+} ions as well as having –COOH groups and $-COO^-$ ions exposed for each adsorbed EDTA molecule. The adsorption mode and self-assembled conformation of EDTA are determined by the interdistance and coordination number of coordinatively unsaturated Ti^{4+} ions on different exposed substrate faces. The HA coating mineralizes on the functionalized surface with the coexistence of two types of microstructural patterns. One is the parallel pattern with the (001) plane preferably parallel to the substrate surface; the other is the radial pattern with [001] preferably radiating from one surface core and (111) preferably parallel to the substrate surface. The mineralization is a result of controlled nucleation under the mechanism of interfacial molecular recognition such as electrostatic interactions, hydrogen bonding interactions, stereochemical arrangements and geometrical correspondence.

5 Acknowledgement

This project was granted financial support from China Postdoctoral Science Foundation.

References

1 F. J. Fendler and F. C. Meldrum, *Adv. Mater.*, 1995, **7**, 607.
2 B. C. Bunker, P. C. Rieke, B. J. Tarasevich, A. H. Campbell, G. E. Fryxell, G. L. Graft, L. Song, J. Liu, J. W. Virden and G. L. McLay, *Science*, 1994, **264**, 48.
3 Q. Huo, H. I. Margolese and G. D. Stucky, *Chem. Mater.*, 1996, **8**, 1147.
4 S. Mann and G. A. Ozin, *Nature*, 1996, **382**, 313.
5 S. Weiner, *CRC Crit. Rev. Biochem.*, 1986, **20**, 365.
6 S. Mann, *J. Mater. Chem.*, 1995, **5**, 935.
7 S. Mann, *Nature*, 1988, **322**, 119.
8 H. B. Lu, C. L. Ma, H. Cui, L. F. Zhou, R. Z. Wang and F. Z. Cui, *J. Cryst. Growth*, 1995, **155**, 120.
9 A. A. Campbell, G. E. Fryxell, J. C. Linehan and G. L. Graff, *J. Biomed. Mater. Res.*, 1996, **32**, 111.
10 C. Ohtsuki, H. Iida, S. Hayakawa and A. Osaka, *J. Biomed. Mater. Res.*, 1997, **35**, 39.
11 H. B. Wen, J. B. de Wijn, Q. Liu, F. Z. Cui and K. de Groot, *J. Mater. Sci. Mater. Med.*, 1997, **8**, 765.
12 R. Pribil, *Analytical Application of EDTA and Related Compounds*, Pergamon Press, Oxford, 1972, pp. 1–50.
13 M. A. Blesa, E. B. Borghi, A. J. G. Maroto and A. E. Regazzoni, *J. Colloid Interface Sci.*, 1984, **98**, 295.
14 E. H. Rueda, R. L. Grassi and M. A. Blesa, *J. Colloid Interface Sci.*, 1985, **106**, 243.
15 H. C. Chang and E. Matijevic, *J. Colloid Interface Sci.*, 1983, **92**, 479.
16 J. Rubi and E. Matijevic, *J. Colloid Interface Sci.*, 1979, **68**, 408.
17 E. B. Borghi, A. E. Regazzoni, A. J. G. Maroto and M. A. Blesa, *J. Colloid Interface Sci.*, 1989, **130**, 299.
18 A. R. Browers and C. P. Huang, *J. Colloid Interface Sci.*, 1986, **110**, 575.
19 A. Ulman, *Chem. Rev.*, 1996, **96**, 1533 and references therein.
20 H. Shin, R. J. Collins, M. R. De Guire, A. H. Heuer and C. N. Sukenik, *J. Mater. Res.*, 1995, **10**, 692.
21 Y. T. Tao, *J. Am. Chem. Soc.*, 1993, **115**, 4350.
22 N. E. Schlotter, M. D. Porter, T. B. Bright and D. L. Allara, *Chem. Phys. Lett.*, 1986, **132**, 93.
23 H. Ogawa, T. Chihara and K. Taya, *J. Am. Chem. Soc.*, 1985, **107**, 1365.
24 Y. T. Tao, M. F. Lee and S. C. Chang, *J. Am. Chem. Soc.*, 1993, **115**, 9547.
25 M. T. Glimcher, *Parodontologie*, 1967, **1**, 55.
26 M. J. Glimcher and S. M. Krane, *Treatise Collagen*, 1965, **2**, 67.
27 M. J. Glimcher, *Annu. Symp. Soc. Gen. Physiol.*, 1959, **6**, 53.
28 M. J. Glimcher, U. A. Friberg, S. Orloff and J. Gross, *J. Ultrastruct. Res.*, 1966, **15**, 74.
29 M. J. Glimcher, B. Lefteriou and D. Kossiva, *Calcif. Tissue. Int.*, 1979, **28**, 83.
30 M. J. Glimcher, *J. Bone Miner. Res.*, 1986, **1**, 509.
31 M. J. Glimcher, D. Kossiva and D. Brickley-Parsons, *J. Biol. Chem.*, 1984, **259**, 290.
32 F. Vigliuni and F. Maroti, *Clin. Ortoped.*, 1963, **15**, 521.
33 M. Mori, M. Ito and S. Fukui, *Histochemie*, 1965, **5**, 521.
34 D. Chapman, *J. Chem. Soc.*, 1955, 1766.
35 R. E. Sievers and J. C. Bailar Jr., *Inorg. Chem.*, 1962, **1**, 174.
36 D. H. Bush and J. C. Bailar Jr., *J. Am. Chem. Soc.*, 1953, **75**, 4574.
37 D. H. Bush and J. C. Bailar Jr. , *J. Am. Chem. Soc.*, 1956, **78**, 716.
38 K. Nakamoto, *Infrared and Raman Spectra of Inorganic and Coordination Compounds*, Wiley & Sons, New York, 1986, 4th edn.
39 R. G. Greenler, *J. Chem. Phys.*, 1966, **44**, 310.
40 J. Umemura, T. Kamata, T. Kawai and T. Takenaka, *J. Phys. Chem.*, 1990, **94**, 62.
41 S. Anderson, E. C. Constable, M. P. Dare-Edwards, J. B. Goodenough, A. Hamnett, K. R. Seddon and R. D. Wright, *Nature*, 1979, **280**, 571.
42 D. L. Parfit, G. D. Russell and V. C. Farmer, *J. Chem. Soc., Faraday Trans. 1*, 1976, **72**, 1082.
43 R. L. Parfitt, G. D. Russell, A. R. Fraser and V. C. Farmer, *Nature*, 1974, **248**, 220.
44 A. D. Buckland, C. H. Rochester and S. A. Topham, *J. Chem. Soc., Faraday Trans. 1*, 1980, **76**, 302.
45 V. E. Henrich and P. A. Cox, *The surface science of metal oxides*, Cambridge University Press, Cambridge, 1994, pp. 280–283, 332–333.
46 H. P. Boehm, *Discuss. Faraday Soc.*, 1971, **52**, 264.
47 I. Nakagawa and T. Shimanouchi, *Spectrochim. Acta*, 1964, **20**, 429.
48 M. Tsuboi, T. Onishi, I. Nakagawa, T. Shimanouchi and S. Mizuschima, *Spectrochim. Acta*, 1958, **12**, 253.
49 R. A. Condrate and K. Nakamoto, *J. Chem. Phys.*, 1965, **42**, 2590.
50 M. Mikami, I. Nakagawa and T. Shimanouchi, *Spectrochim. Acta*, 1967, **23**, 1037.
51 C. D. Wagner, W. M. Riggs, L. E. Davies, J. F. Moulder and G. E. Muilenberg, *Handbook of X-ray photoelectron spectroscopy*, Perkin-Elmer Corporation, Eden Prairie, MN, 1979, pp. 58–70.
52 C. N. Sayer and N. R. Armstrong, *Surf. Sci.*, 1978, **77**, 301.
53 E. Bertel, R. Stockbauer and T. E. Mady, *Surf. Sci.*, 1984, **141**, 355.
54 D. E. Eastman, *Solid State Commun.*, 1972, **10**, 933.
55 K. I. Hadjiivanov and D. G. Klissurski, *Chem. Soc. Rev.*, 1996, **25**, 61.
56 T. Hanawa, M. Kon, H. Ukai, K. Murakami, Y. Miyamoto and K. Asaska, *J. Biomed. Mater. Res.*, 1997, **34**, 273.
57 G. Beamson and D. Briggs, *High Resolution XPS of Organic Polymers, the Scienta ESCA300 Database*, John Wiley & Sons, New York, 1992, pp. 66, 116.
58 G. M. Whitesides, J. P. Mathias and C. T. Seto, *Science*, 1991, **254**, 1312.
59 R. J. Fessenden and J. S. Fessenden, *Organic Chemistry*, Brooko/Cole Publishing Company, California, 1986, 5th edn., pp. 64–65, 584–585.
60 J. A. Dean, *Lange's Handbook of Chemistry*, Mc-Graw-Hill Book Company, New York, 14th edn, 1992.
61 Th. Zeegers-Huyskens and P. Huyskens, *Intermolecular forces*, in *Intermolecular forces, an Introduction to Modern Methods and Results*, ed. P. L. Huyskens, W. A. P. Luck and T. Zeegers-Huyskens, Springer-Verlag, Berlin, 1991, pp. 17–29.
62 C. B. Mao, H.D. Li, F. Z. Cui, Q. L. Feng, H. Wang and C. L. Ma, *J. Mater. Chem.*, 1998, **8**, 2795.
63 M. M. Walczac, C. Chung, S. M. Stole, C. A. Nidrig and M. D. Porter, *J. Am. Chem. Soc.*, 1991, **113**, 2370.
64 J. H. Keeler, W. R. Hibbard and B. F. Decker, *Trans. AIME*, 1953, **197**, 932.
65 M. Kukura, L. C. Bell, A. M. Posner and J. P. Quirk, *J. Phys. Chem.*, 1972, **76**, 900.
66 M. Tanahashi and T. Matsuda, *J. Biomed. Mater. Res.*, 1997, **34**, 305.
67 A. S. Posner, F. Betts and N. C. Blumenthal, *Prog. Cryst. Growth Charact.*, 1980, **3**, 49.
68 T. Hanazawa, *Inorganic Phosphate Materials*, Elsevier, Amsterdam, 1989, pp. 24–29, 91–92.

Paper 9/01309A